Peak Detection in Intracranial Pressure Signal Waveforms: A Comparative Study

Miaomiao Wei
Zhongyuan University of Technology
Solventa Krakauskaite
Pepperdine University
Sreya Subramanian
Pepperdine University
Fabien Scalzo (fabien.scalzo@gmail.com)
University of California, Los Angeles

Research Article

Keywords:

Posted Date: May 18th, 2023

DOI: https://doi.org/10.21203/rs.3.rs-2909348/v1

Additional Declarations: No competing interests reported.

Peak Detection in Intracranial Pressure Signal Waveforms: A Comparative Study

Miaomiao Wei[1], Solventa Krakauskaite[3], Sreya Subramanian[3], Fabien Scalzo[2,3,*]

[1]Department of Electronic and Information, Zhongyuan University of Technology, Zhengzhou, China

[2]Department of Neurology, University of California, Los Angeles (UCLA), USA

[3]Seaver College, Pepperdine University, Malibu, USA

[*]Corresponding author, email address: fabien.scalzo@gmail.com

Abstract

Background: The monitoring and analysis of quasi-periodic biological signals such as electrocardiography (ECG), intracranial pressure (ICP), and cerebral blood flow velocity (CBFV) waveforms plays an important role in the early detection of adverse patient events and contributes to improved care management in the intensive care unit (ICU). This work provides a quantitative evaluation of existing computational frameworks for the automatic extraction of peaks within ICP waveforms.

Methods: Peak detection techniques based on state-of-the-art machine learning models were evaluated in terms of robustness to varying levels of noise. Evaluation was performed on a dataset of ICP signals assembled from 700 hours of monitoring from 64 neurosurgical patients. The groundtruth of the peak locations was established manually on a subset of $13,611$ pulses. Additional evaluation was performed using a simulated dataset of ICP with controlled temporal dynamics and noise.

Results: The quantitative analysis of peak detection algorithms applied to individual waveforms indicates that all techniques provide acceptable accuracy (RMSE ≤ 0.15) without noise. In presence of higher level of noise, however, only Kernel ridge regression and Random forest remains below that error threshold while the performance of other techniques significantly deteriorates. Our experiments also demonstrated that tracking methods such as Bayesian inference and LSTM can be applied in a continuous fashion and provide additional robustness in situations where single pulse analysis methods tend to fail such as in presence of missing data.

Conclusion: While machine learning-based peak detection methods require manually labeled data for training, these models outperform conventional signal processing ones based on handcrafted rules and should be considered for peak detection in modern frameworks. In particular, peak tracking methods that incorporate temporal information between successive periods of the signals have demonstrated in our experiments to provide more robustness to temporary artifacts that commonly arise as part of the monitoring setup in the NICU.

I. Introduction

The monitoring of quasi-periodic biological signals such as arterial blood pressure (ABP), intracranial pressure (ICP), and electrocardiography (ECG) plays a fundamental role in the study of numerous disorders and diseases. These biological signals have something in common; they all exhibit characteristic variations that can be used by clinicians as markers of physiological change and provide additional insights through further analyses. This comparative study focuses on the ICP waveform which is a quasi-periodic signal. As visualized in Figure 1, each pulse can be associated with three peaks due to its triphasic nature [1]. Therefore, ICP morphological analysis often relies on the identification of these three peaks. Based on their latency (*i.e.*, time) and elevation (*i.e.*, height), it is possible to characterize the morphology over time and then compute statistics of the ICP waveform for a particular time interval. We provide in this paper a comparative analysis of techniques for the detection of the three peaks across the periods of the signal.

The study of the variations of the ICP signal is particularly important for patients of the NICU treated for traumatic injury (TBI) as the morphological variations observed in the ICP waveform may reveal the compensatory ability of the brain in presence of cerebrovascular disruptions. Several computational frameworks have been developed to study how the changes observed in the morphology of the ICP signal are associated with the development of cerebral vasospasm [2], intracranial hypertension [3, 4], and abrupt changes in the cerebral blood carbon dioxide (CO2) levels [1, 5], and changes in the craniospinal compliance [6]. In addition to average change of the ICP, studies [7, 8] have linked the morphology of the ICP waveforms with the prognosis of patients with a head injury. Hence, exploring ICP morphological characteristics such as peaks may help monitor pathophysiological intracranial changes.

Traditionally, peak detection in biological signals has been achieved using signal processing methods, including threshold-based and filtering methods [9], [10]. More recently, machine learning (ML)-based methods [11], [12] have been developed to solve this problem. ML methods are usually built on top of signal processing methods to obtain more robustness to noise by capturing the characteristics of the peaks and adapting to the noise profile of the signal that is specific to the context in which it is acquired. There exists a wide range of machine learning models available, including Neural Network, Random Forest, support vector machines (SVM), long short-term memory (LSTM), etc. In the context of ICP analysis, these models can be

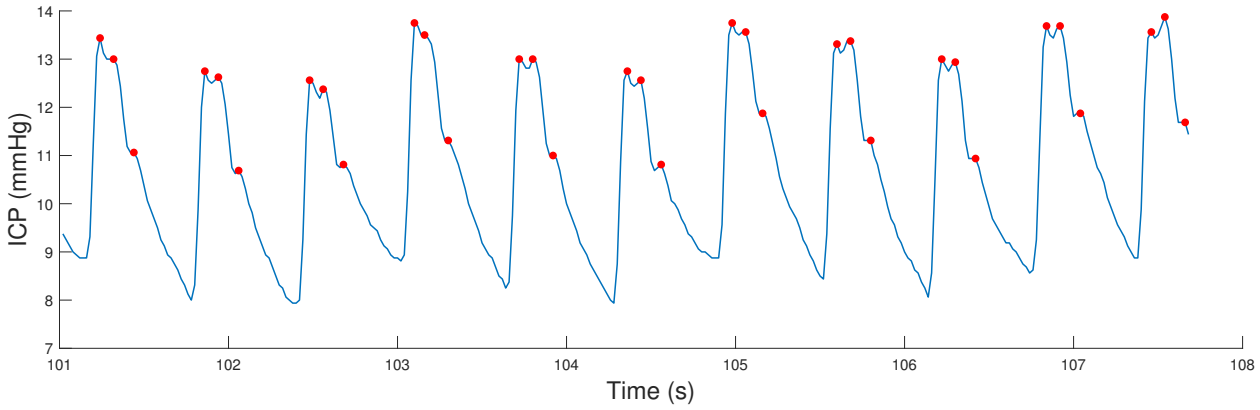

Fig. 1: Example of continuous real-time monitoring of ICP waveform from a patient in the NICU. The three peaks within each triphasic waveform are depicted by red dots.

grouped into two main categories depending if they are processing a single pulse at a time, or if they are processing the continuous signal instead. It remains unclear, however, which methods are the best performing ones on ICP signals.

In this study, we provide a comparative study of ICP peak detection methods. After a technical review and description of the literature, we describe our peak detection experiments performed on real and simulated ICP datasets.

II. State-of-the-art

A. *Summary*

Peak detection techniques can be grouped into two categories depending if they are processing individual waveforms or if, instead, they are utilizing temporal patterns from previous waveforms to identify peaks in the current waveform. Traditionally, peak detection on individual waveforms has been achieved using signal processing techniques. In that scenario, it is common to assume that a peak is simply a local extrema of the curvature of the signal. In the context of peak detection in biomedical signals such as ICP, however, the presence of artifacts and noise makes the recognition of peaks very challenging when only relying on signal processing methods. To tackle this problem, researchers have developed peak detection techniques based on machine learning. These techniques have demonstrated significant promises to provide more robust detection of peaks in biomedical signals.

Because strong correlation may exist between the peak locations of successive waveforms, tracking techniques such as Kalman filter, LSTM, Bayesian inference, or MOCAIP can be used

to capture the temporal information between successive pulses to refine the location of the peaks. We review in the following sub-sections the techniques available in the literature to perform peak detection on individual (Section II-B) and continuous (Section II-C) waveforms.

B. Peak detection on individual waveforms

Peak detection is assumed here to be performed on individual ICP pulses previously segmented from continuous ICP waveforms [10, 13]. In particular, we divide the individual pulses methods into two sub-groups depending if they are based on signal processing only or if they utilize machine learning models during processing.

1) Signal-processing techniques: In signal processing, it is common to think of peak detection as a search for a local extrema in the curvature of the signal. Most of signal-based methods utilize the local structure of the signal to identify the peaks. Among them, we identify threshold-based processes [14, 15], derivative-based techniques [16], and transform domain techniques [17–19]. Other methods perform peak detection by incorporating a larger context to describe the signature of each peak within the beat, which includes intensity weighted variance [20], filter-based techniques [21, 22], histogram-based techniques [23, 24], techniques using entropy [25], momentum [26], stochastic resonance [27], higher-order statistics [28], nonlinear energy operator [29], empirical mode decomposition [30]. More advanced techniques such as the wavelet transform and entropy of coefficients [31, 32] have also achieved promising results.

While peak detection techniques purely based on signal processing perform well on a wide range of applications, they encounter significant challenges when applied to real-world ICP data due to the variability across subjects, motion artifacts, and hardware acquisition noise that is characteristic of ICP waveforms. These challenges have pushed researchers to utilize techniques that are more robust to these variations, as described in the next sub-section.

2) Machine learning-based techniques: Machine learning-based methods formalize peak detection as a regression analysis problem between the input ICP waveform and the location of each peak. This section gives an overview of ML methods that have been used to detect ICP peaks and will be evaluated in our experiments. These methods include Spectral Regression (SR) [33], Neural Networks (NN) [34], Support Vector Machines (SVM) [35], and Extremely Randomized Decision Trees (Extra-Trees) [36].

Spectral Regression (SR). The SR algorithm [33] is an nonlinear regression method that incorporates graph-based analysis with linear regression. The objective is to learn a regression

model that outputs similar predictions $\hat{y}_i$ for input samples x_i that are near each other in a graph representation. The regression model is obtained by minimizing the following measure ϕ:

$$\phi = \sum_{i,j=1}^{n} (\hat{y}_i - \hat{y}_j)^2 \, W_{i,j} \tag{1}$$

where $W_{i,j}$ is the affinity matrix $W \in \mathbb{R}^{n \times n}$ that assigns a value to $W_{i,j}$ to indicate the similarity of the two input samples x_i, x_j.

During learning, SR searches for vectors $\{\hat{\alpha}_0, \hat{\alpha}_1, \ldots, \hat{\alpha}_d\}$ to minimize the remaining Sum of Square Error (SSE),

$$\hat{\alpha_j} = \text{argmin}_\alpha \sum_{i=1}^{n} (\alpha^T x_i - y_i^j)^2 \tag{2}$$

where y_i^j signifies the i-th element of the j-th eigenvector e_j of the affinity matrix W.

Though SR is proposed to solve linear problems, it can be extended to nonlinear problems through a kernel projection, which projects the original observation x_i into a higher dimensional using a nonlinear kernel. In the kernel version, refered to as Kernel Spectral Regression (KSR), the observations x_i in Eq.(2) are replaced by the projected vectors in Eq.(3). In this study, we use the Radial Basis Function (RBF) kernel,

$$R(x_i, x_j) = \exp(-\beta ||x_i - x_j||^2), \ \beta > 0 \tag{3}$$

Neural Networks (NN). Neural networks is another very popular machine learning model that can be used to infer peak locations from an ICP waveform. Numerous neural networks architectures exist, we focus here on a feed-forward network that comprises input, hidden, and output layers. The Levenberg-Marquardt algorithm [37] was used for its efficiency in training moderate-sized NNs. The SSE is used as the fitness function V:

$$V = \sum_{i=1}^{N} (x_{i_{out}} - x_{i_{in}})^2 \tag{4}$$

where $e_i = x_{i_{out}} - x_{i_{in}}$ is the bias between outputs and inputs, N is the number of inputs.

Supper Vector Machine (SVM). A support vector machine (SVM) [35] is a supervised learning method that constructs a set of hyperplanes in a high-dimensional space. SVM has been proven to be an effective tool in real-value function estimation. In the context of regression, SVM (also called support vector regression (SVR)) uses a n-dimensional tube to fit the data. During learning, the optimization process adopts an ϵ-insensitive loss function, penalizing predictions that are farther than the threshold ϵ from the desired output. The value of ϵ determines the diameter

of the tube; a smaller value indicates a lower tolerance for error and affects the smoothness of the overall predictions. For regression problems, the goal of SVM is to identify the parameters of a set of hyperplane(s)/tube(s) that best fit the data. After training, a prediction can be obtained for a new input vector x_j,

$$f(x) = \sum_{i=1}^{n} (\alpha_i^+ - \alpha_i^-) R(x, x_j) + b \tag{5}$$

where α^+, α^- represents the learned dual coefficients, $R(x, x_j)$ is the response of the RBF kernel (Eq. 3) of the point x_j, and b is the bias.

Extremely Randomized Decision Trees (Extra-Trees). Extra-Trees [36] is a regression method based on an ensemble of randomized decision trees. The learning of a randomized decision tree is performed by starting at the root node of the tree and successively splitting its left and right sub-trees. Each split (i.e. threshold) is obtained by sampling according to a Gaussian distribution estimated from the training samples. The process is repeated iteratively until a node has constant output values for all the training inputs. By building a large number of randomized decision trees (e.g. $N > 100$), the model can make predictions by using a new input through each tree and computing the average prediction across all the trees.

C. Peak Tracking on Continuous Waveforms

Although peak detection on individual pulses can achieve reasonable accuracy by either identifying the signal signature of these peaks or learning a regression model between the waveform and the peak location with machine-learning, processing individual pulses has some limitations. Hardware noise and human disturbance (such as motion artifacts) are inevitable in a clinical environment. These may cause distortion or even temporary loss of ICP waveform, making it challenging to detect and track peaks over time based solely on a single pulse. Achieving continuous and real-time analysis of ICP waveforms is a high-level requirement of ICP monitoring in the NICU. We provide here a description of techniques that have been developed to process the continuous ICP signal and locate the peaks using temporal properties between successive beats as prior information, effectively tracking them across different periods. In the following, we describe Kalman filtering [38], Bayesian tracking [39], and LSTM [40], and MOCAIP [41].

Kalman filtering. The Kalman filter algorithm [42] is a recursive algorithm that estimates the distribution of unknown variables from the measured noisy data. After several iterations, the estimated value is expected to converge to the actual value of the unknown variables; the location of the peaks in our case. The process is efficient as it only needs the current measured input, the previous state, and the uncertainty state matrix to calculate the predicted value when the subsequent measurement is observed. The Kalman filter is composed of a prediction and an updating step.

During the prediction step, the state variable $\hat{x}_k^-$ and its covariance P_k are predicted.

$$\hat{x}_k^- = A\hat{x}_{k-1} + Bu_k \tag{6}$$

$$P_k^- = AP_{k-1}A^T + Q \tag{7}$$

where A is the state-transition matrix, B is the control-input model, and Q represents the covariance of the noise.

During the updating step, these estimates are evaluated using a weighted average, such that a greater weight is set to estimations with greater confidence,

$$K_k = P_k^- H^T (HP_k^- H^T + R) + Q^{-1} \tag{8}$$

$$\hat{x}_k = \hat{x}_k^- + K_k(z_k - H\hat{x}_k^-) \tag{9}$$

$$P_k = (I - K_k H)P_k^- \tag{10}$$

where H represents the observation matrix, $\hat{x}_k^-$ and $\hat{x}_k$ are the prior and posterior state estimates at step k. z_k and u_k are the measurements and the control vectors at step k, and K represents the Kalman filtering gain.

Bayesian tracking. Nonparametric belief propagation (NBP) [43] is a probabilistic inference algorithm applied in computer vision to track the movements of people, animals, robots, cars, etc. We previously used NBP [39] to track ICP peaks in real-time. Bayesian inference associates continuous probability distributions as the location of each peak.

During detection, NBP utilizes a dynamic graph where nodes represent the location of each peak. Information between the different peaks of a current pulse, and between the peaks at the prior time point are progapated in the graph via a message-passing algorithm called Belief propagation. At the n-th iteration, the message m passed from node a to b is expressed as:

$$m_{a,b}^n(x_a) \leftarrow \int \phi_{a,b}(x_a, x_b)\phi_a(x_a, y_a) \prod_{c \in C_{a \setminus b}} m_{c,a}^{n-1}(x_a) dx_a \tag{11}$$

where $x_a \in \mathbf{x}$ represents the hidden variable at node a. $C_{a\backslash b}$ represents the set of nodes connected to a (except node b). $\phi_a(x_a, y_a)$ is the observation potential between hidden variable x_a and observation variable y_a of node a, $\phi_{a,b}(x_a, x_b)$ is the compatibility potential between hidden variables x_a and x_b. After several iterations, the approximation of nth iteration $\hat{p}^n(x_a|y)$ converges to the true marginal distribution $p(x_a|y)$ is:

$$p(x_a|y) \sim \hat{p}^n(x_a|y) \leftarrow \phi_a(x_a, y_a) \prod_{b \in C_a} m^n_{a,b}(x_a) \tag{12}$$

In NBP, the message $m_{a,b}(x_a)$ is expressed as a mixture of D kernels:

$$m_{a,b}(x_a) = \frac{1}{D} \sum_{i=1}^{D} \omega^i_a N(x_a; \mu^i_a, \Sigma^i_a) \tag{13}$$

where ω^i_a is the weight of the *i-th* kernel with mean μ^i_a and variance Σ^i_a. D is the number of particles used for estimation. The observation potential is represented as weighted mixtures of Gaussian density functions.

Long short time memory (LSTM). LSTM [40] is a type of recurrent neural network (RNN) which allows information to persist inside the network via loops in its architecture. LSTMs are particularly well suited to represent time series such as ICP waveforms. A LSTM cell is defined by a state that changes according to three types of gates:

- Input Gates $i_t \in \mathcal{R}^N$ update the state of the cell and decide which values should be updated.
- Forget Gates $f_t \in \mathcal{R}^N$ are used to select relevant information with respect to a previous state.
- Output Gates $o_t \in \mathcal{R}^N$ determine the final cell state and the output value.

Given an input sequence $x = \{x_1, x_2, \ldots, x_T\}$ of length T with corresponding memory cell unit $C_t \in \mathcal{R}^N$ and hidden unit $h_t \in \mathcal{R}^N$ at time t, the parameters of the model are updated sequentially, as follows:

$$f_t = \sigma(W_f.[h_{t-1}, x_t] + b_f) \tag{14}$$

$$i_t = \sigma(W_i.[h_{t-1}, x_t] + b_i) \tag{15}$$

$$o_t = \sigma(W_o[h_{t-1}, x_t] + b_o) \tag{16}$$

$$\tilde{C}_t = \tanh(W_c.[h_{t-1}, x_t] + b_C) \tag{17}$$

$$C_t = f_t * C_{t-1} + i_t * \tilde{C}_t \tag{18}$$

$$h_t = o_t * \tanh C_t \tag{19}$$

The function $\sigma(x) = (1 + e^{-x})^{-1}$ used to compute f_t, i_t, o_t is a sigmoid whose values lie within the range $[0, 1]$. In addition to input, forget, and output gates previously described, the LSTM makes use of a memory cell unit C_t obtained from the sum of the previous memory cell unit C_{t-1} modulated by f_t, and a function of the current input x_t and previous hidden state h_{t-1} modulated by the input gate i_t. The output gate o_t is then used to determine what parts should be considered and then multiplied with the $\tanh$ of the memory cell state C_t to produce the hidden unit h_t. By learning how much of the memory cell state C_t should be transferred to the hidden state h_t based on the input x_t and previous state, this structure allows the LSTM to capture complex temporal dynamics such as the ones present across ICP waveforms.

MOCAIP algorithm. The Morphological Clustering and Analysis of ICP Pulse (MOCAIP) [41] framework was designed to extract morphological variations of ICP pulses. MOCAIP utilizes a Gaussian distribution as prior model for the peak location. The detection of ICP peaks is performed through the three main following steps:

- Pulse segmentation: The continuous ICP signal is segmented into a series of individual pulses using a dedicated algorithm [44] that utilizes ECG QRS markers [45]. A hierarchical clustering algorithm is utilized to extract a representative pulse over a segment of 1 minute.
- Peak candidates detection. Candidate peaks are detected on the ICP pulse using its second derivative. They are extracted from the convex region and the concave region on the ascending edge of the signal or the concave part and the convex part on the falling edge of the signal.
- Peak Designation. The three peaks are selected from the set of candidate peaks such that they maximize the likelihood to belong to a previously trained Gaussian mixture model (i.e. prior model).

III. Results

A. Experiment #1: Peak Detection in Individual Waveforms

The RMSE of six peak detection algorithms on individual waveforms is reported in Table I after a 10-fold cross-validation. The table summarizes the results for each of the three peaks. Each sub-table corresponds to the performance with respect to one of the peaks. The fourth sub-table represents the average performance across all peaks. The columns correspond to the different noise levels (from 0 to 15%). The RMSE values were mapped to a color such that blue indicates lower error, and yellow indicates higher error.

On average, the results on the clinical dataset shows that the error is the smallest for p_2, followed by p_1, and finally, p_3. This is because the position of p_2 is more stable than other peaks. In the absence of added noise, KSR, LSTM, and Random forests perform best (RMSE = 0.08) when considering the average of the three peaks. In the presence of noise, the estimated error of KSR is the smallest (RMSE = 0.13) as it appears to be less affected by noise. As expected, the RMSE of all algorithms increase as a result of the noise level. We note that all algorithms do not grow at the same rate with respect to the noise. For example, the error of Spectral/Ridge regression and Neural network increase at a rate much higher that other methods which might indicate over-fitting.

Similarly, Table II provides the results after evaluating the peak detection methods on the simulated dataset. When the error is averaged over the three peaks, KSR offers the best performance among the six algorithms regardless of the level of noise. The RMSE of Spectral/Ridge regression, LSTM, Neural network, and Random forests are significantly higher (RMSE ≥ 0.29) and are greatly affected by noise. From the results summarized in Table I and Table II, we conclude that KSR performs better than the other algorithms.

B. Experiment #2: Peak detection in Continuous ICP

The results of the peak tracking methods (Bayesian tracking, Kalman Filter, LSTM, and MOCAIP) on continuous ICP are illustrated in Figure 2 and Figure 3. In Figure 2, each plot includes the latency of the peak with noise (gray) and the filtered position of the tracking algorithm (color curves). These curves are repeated for each of the three peaks (p_1, p_2, and p_3), which can be judged according to the value range of its Y-axis. Figure 3 displays the results in terms of the elevation of the first peak. For better visibility, we opted to only show the tracking of the first peak as all peaks tend to be within the same elevation range in our simulated dataset.

The accuracy of each tracking algorithm can be observed based on how close the estimate is from the groundtruth (shown in Figure 6 (b)). The tracking results of the Bayesian tracking and Kalman filtering framework on the three peaks closely follows the original peak latency. Although the signal is affected by noise, the tracking results still reflect the trend of the original position very well. We can conclude that the tracking algorithm effectively tracked the continuous waveform under this noise setting (i.e. 5%). The tracking result of LSTM is not so consistent with the grountruth location, and its tracking result behaves differently for each peak and in different periods. The tracking result of p_1 is better than that of p_2 and p_3. For p_3, the detection

Peak 1	Noise 0%	Noise 5%	Noise 10%	Noise 15%
Ridge Regression	0.13	0.15	0.19	0.25
Kernel Ridge Regression	0.10	0.11	0.13	0.16
SVM	0.09	0.11	0.19	0.23
LSTM	0.15	0.13	0.15	0.20
Neural Network	0.11	0.32	0.44	0.53
Random Forests	0.09	0.11	0.13	0.15

Peak 2	Noise 0%	Noise 5%	Noise 10%	Noise 15%
Ridge Regression	0.12	0.23	0.43	0.63
Kernel Ridge Regression	0.07	0.07	0.08	0.11
SVM	0.07	0.09	0.14	0.17
LSTM	0.12	0.13	0.15	0.17
Neural Network	0.09	0.16	0.19	0.22
Random Forests	0.09	0.10	0.12	0.13

Peak 3	Noise 0%	Noise 5%	Noise 10%	Noise 15%
Ridge Regression	0.10	0.16	0.25	0.36
Kernel Ridge Regression	0.07	0.08	0.10	0.12
SVM	0.07	0.10	0.17	0.22
LSTM	0.12	0.14	0.16	0.19
Neural Network	0.09	0.36	0.53	0.62
Random Forests	0.07	0.12	0.16	0.19

All Peaks	Noise 0%	Noise 5%	Noise 10%	Noise 15%
Ridge Regression	0.12	0.18	0.29	0.42
Kernel Ridge Regression	0.08	0.09	0.10	0.13
SVM	0.08	0.10	0.17	0.20
LSTM	0.13	0.13	0.15	0.18
Neural Network	0.10	0.28	0.39	0.45
Random Forests	0.08	0.11	0.14	0.16

TABLE I: Performance of peak detection algorithms in terms of RMSE after evaluation on clinical ICP data with varying noise levels (from 0 to 15%).

is poor at the beginning and end of the tracking. The inconsistency in the initial part could be caused by the initialization phase of the LSTM. Finally, the tracking result of MOCAIP captures the overall variations of the peak location but does not offer the same level of granularity than other techniques. This is because MOCAIP is based on a clustering process to achieve peak detection. The input data is obtained by using a 1-min cluster average. However, it is worth mentioning that MOCAIP does not require a training process.

1) Missing data: The tracking results in presence missing data are illustrated in Figure 4, where the blue curve represents the waveform with missing segments, and the red represents

Peak 1	Noise 0%	Noise 5%	Noise 10%	Noise 15%
Ridge Regression	0.25	0.35	0.47	0.61
Kernel Ridge Regression	0.25	0.26	0.28	0.32
SVM	0.26	0.23	0.26	0.33
LSTM	0.27	0.27	0.27	0.27
Neural Network	0.22	0.33	0.33	0.33
Random Forests	0.27	0.28	0.28	0.28

Peak 2	Noise 0%	Noise 5%	Noise 10%	Noise 15%
Ridge Regression	0.10	0.11	0.12	0.13
Kernel Ridge Regression	0.07	0.07	0.07	0.08
SVM	0.10	0.11	0.11	0.13
LSTM	0.24	0.29	0.36	0.45
Neural Network	0.27	0.33	0.33	0.33
Random Forests	0.30	0.30	0.29	0.30

Peak 3	Noise 0%	Noise 5%	Noise 10%	Noise 15%
Ridge Regression	0.14	0.14	0.14	0.14
Kernel Ridge Regression	0.12	0.13	0.14	0.16
SVM	0.14	0.15	0.15	0.16
LSTM	0.18	0.18	0.18	0.18
Neural Network	0.24	0.31	0.31	0.32
Random Forests	0.26	0.27	0.27	0.28

All Peaks	Noise 0%	Noise 5%	Noise 10%	Noise 15%
Ridge Regression	0.16	0.20	0.24	0.29
Kernel Ridge Regression	0.15	0.15	0.16	0.18
SVM	0.17	0.16	0.18	0.21
LSTM	0.23	0.24	0.27	0.30
Neural Network	0.24	0.32	0.32	0.33
Random Forests	0.28	0.28	0.28	0.29

TABLE II: Performance of of peak detection algorithms in terms of RMSE after evaluation on simulated ICP waveforms with varying noise levels (from 0 to 15%).

the inferred output using one of the tracking algorithms. To enhance contrast, only tracking results for the missing data are displayed. The missing data segments are randomly distributed in the whole waveform range. In most cases, the tracking algorithm recovers the missing data by effectively capturing the trend of the data.

By observing the output predictions of the MOCAIP algorithm, we can see it can approximate the trend of the peak position even when data was missing. Although MOCAIP does not follow the details of the changes, it is still useful to get an approximate estimation for missing data segments. On the other hand, LSTM provides a more refined estimate of the missing data. It

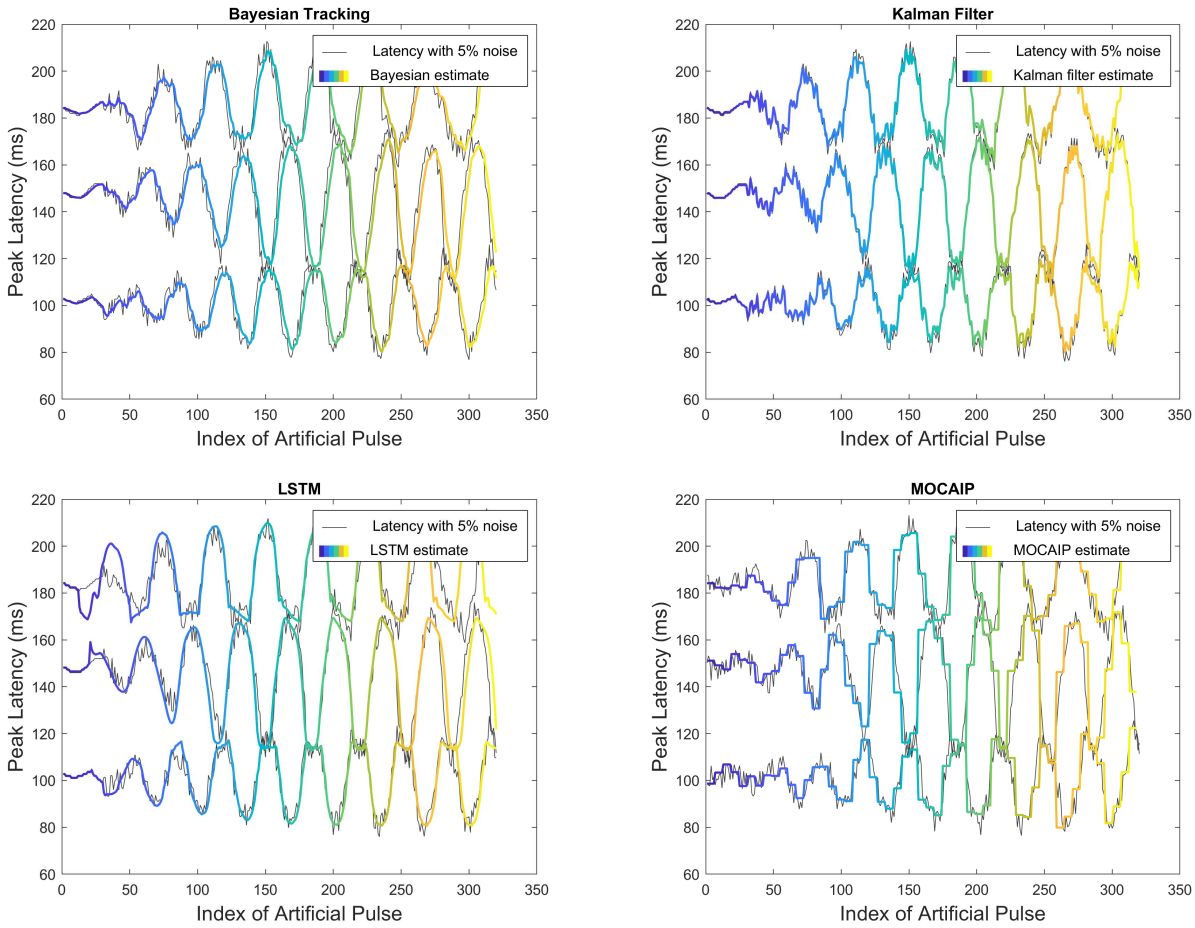

Fig. 2: Tracking result on an simulated ICP dataset with 5% additive noise. Color curves represent the filtered peak latency on our simulated dataset using 4 different tracking models: Bayesian tracking, Kalman filter, LSTM, MOCAIP.

should also be pointed out that only LSTM and MOCAIP algorithms are used for missing data simulation because both Bayesian tracking and Kalman filter frameworks rely on the input for tracking, and the frameworks will not work when no input data is provided.

IV. Discussion

Over the last two decades, machine learning algorithms have produced significant breakthrough in a wide range of domains. We demonstrated in this study the ability of several machine learning models to achieving high accuracy in a peak detection problem on a quasi-periodic signal; the intracranial pressure signal (ICP). Among the evaluated techniques, the peak detection error

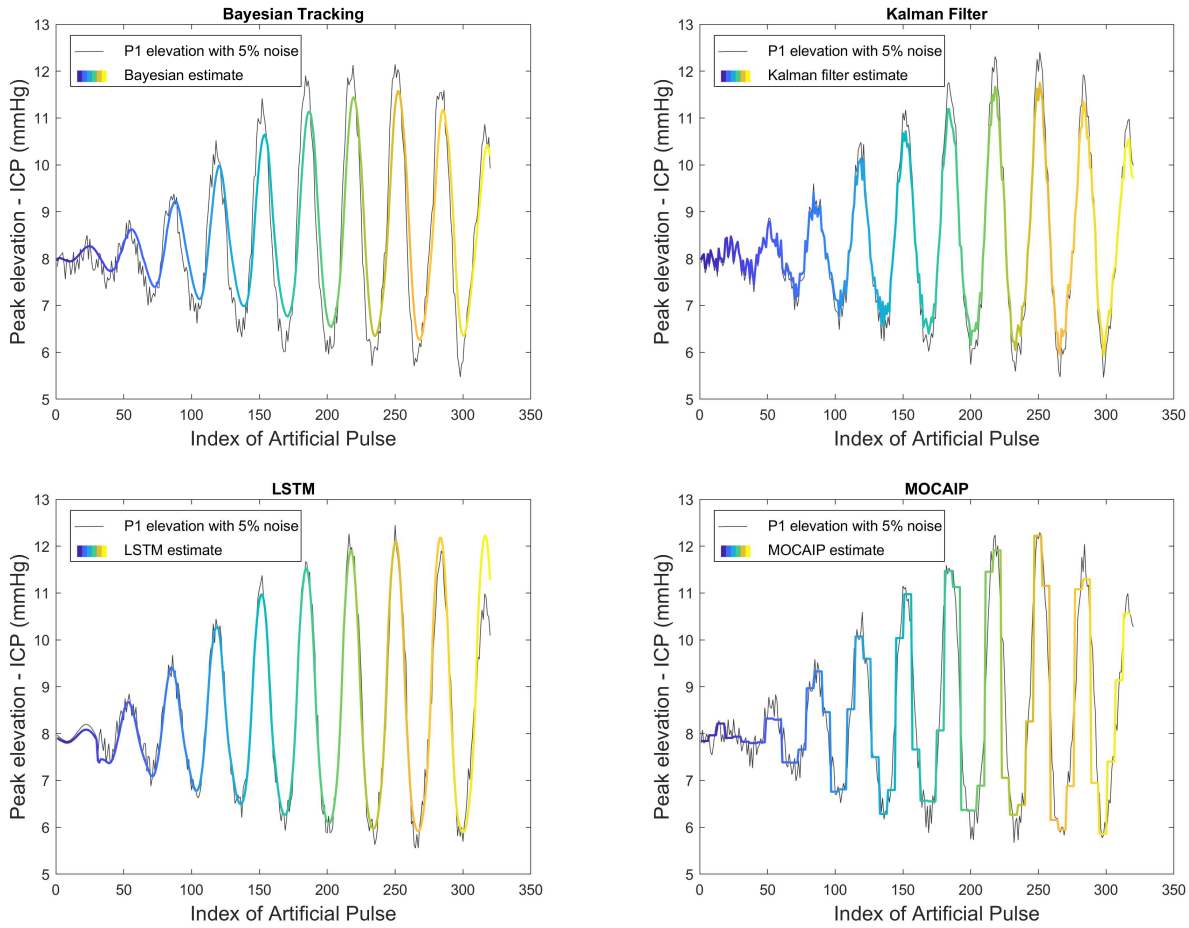

Fig. 3: Tracking result on an simulated ICP dataset with 5% additive noise. Color curves represent the filtered elevation of the first peak on our simulated dataset using 4 different tracking models: Bayesian tracking, Kalman filter, LSTM, MOCAIP.

of Kernel spectral regression (KSR) was the lowest, whether based on simulated or clinically acquired data.

We provided comparative results regarding tracking methods used to perform continuous filtering of the peaks. Bayesian inference, Kalman Filtering, LSTM and MOCAIP algorithms can be used to incorporate the temporal dependence of neighboring pulses in the peak prediction process. The results of our experiments show that such frameworks are particularly robust to noise and missing data.

ICP pulses arise from the blood pressure variation in the cerebral vasculature. In an ICP pulse, the specific distribution of sub-peaks is affected by capillary, arterial, and venous blood pressure pulses and their interactions with three major intracranial parts, including the brain

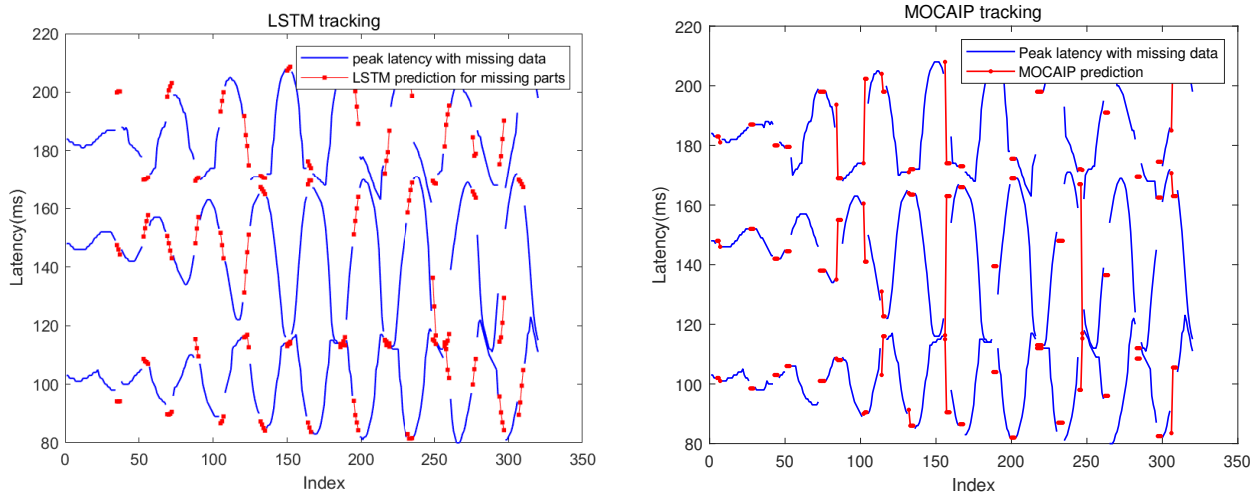

Fig. 4: Tracking result of peak waveform with 5% noise added (blue represents the peak waveform with noise, green represents the original peak waveform, and red represents the simulation result of the tracking algorithm).

tissue, the cerebral vasculature, and the cerebrospinal fluid circulatory system. Consequently, it is conceivable that ICP pulse morphological changes may provide reasonable indications of changes in these compartments. Also, these changes can be triggered by various pathological incidents, such as the narrowing cerebral arteries (vasospasm) after subarachnoid hemorrhage and the development of mass-occupying lesions after a brain injury. Therefore, the long-term continuous monitoring and recording of the ICP waveform provide the changing trend of the patient's physical condition, which is helpful for doctors to conduct pathological analysis of the state. Moreover, the tracking algorithm can predict the position of the ICP peak in a short period, which is also helpful for predicting the development of the disease in the clinical setting. In addition, given the interaction between biological signals, further study on the relationship between ICP and other biological signals to assist ICP waveform analysis is another direction to improve peak detection technology.

All the data and code used as part of our experiment will be made publicly available on the lab website of Prof. Scalzo (http://www.fabiens.net). To the best our knowledge, this would become the first publicly available and curated dataset of ICP signals with both simulated and clinical sources. This is provided with the hope that the data and experimental protocol can serve a as benchmark for the development and evaluation of future peak detection methods in ICP.

V. Conclusion

This paper demonstrates that tracking of ICP waveform morphology can be performed in real-time with high accuracy using machine learning models such as Kernel spectral regression (KSR), Support vector machine (SVM), and LSTM. The acquisition of the ICP signal in a neuro-intensive care unit (NICU) is often associated with signal loss and severe artifacts. To address these issues, our study demonstrated that peak detection models can be coupled with tracking models such as Kalman filter and Non-parametric Bayesian inference to obtain robustness to temporary signal loss. Although these tracking frameworks are demonstrated on ICP waveforms, they could in principle be used as part of the detection process of other quasi-periodic biological signals, such as ECG and CBFV.

VI. Methods

A. Problem formulation

When acquired at a high enough frequency, ICP signals typically exhibit a sequence of waveform pulses such that each pulse includes three peaks, as illustrated in Figure 5. We decompose the peak detection process on a raw signal by assuming that the continuous ICP waveform has been segmented into a set of individual beats $(s_1, s_2, \ldots, s_n)$ using a standard beat segmentation algorithm [10, 13]. This is generally achieved with very high accuracy - especially when the ECG signal is available. Assuming a segmented ICP waveform, we focus on two formulations of the problem of peak detection. In the first case, we consider the task of detecting the three peaks within a single ICP pulse. In the second case, the peak detection is achieved by a tracking algorithm that exploits the estimated position of the peaks from previous pulses. In both formulations, a peak location is defined in terms of its temporal location $l \in \mathcal{R}$ and intracranial pressure elevation $e \in \mathcal{R}$, such that $p_{i\in 1,2,3} = \{l, e\}$ denotes the i-th peak of the pulse. The goal is to obtain automatically the position of the peaks in each beat s_i using a peak detection algorithm P_d, which can be denoted as $P_d(s_i) = \{p_1, p_2, p_3\}$.

B. ICP Data

1) Clinical dataset: The dataset of ICP signals used in this study was collected from 64 patients receiving treatment for various ICP-related disorders in the NICU. Acquisition of the ICP was achieved using intraparenchymal microsensors placed in the right frontal lobe. The

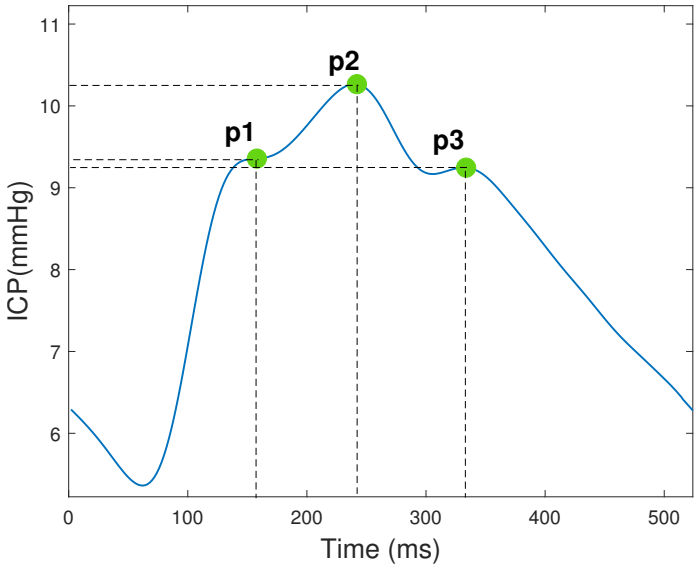

Fig. 5: Illustration of a segmented pulse from a continuous ICP waveform and its three peaks (p1, p2, p3).

raw ICP waveform was recorded continuously at a sample rate of either 240Hz or 400Hz. 153 segments of ICP signal lasting almost five hours were extracted. ICP and ECG signal were then pre-processed to segment individual beats to produce a set of 14,230 raw pulses. Among them, 13,611 valid pulses were obtained and formed the clinical dataset used for our simulation. The dataset is particularly challenging because there is a large variability in the ICP signals due to the condition of each patient.

Three experienced researchers established the groundtruth by reviewing each ICP pulse and manually assigning the position of the three peaks. Specifically, the task of the researcher was to select the right peak candidates for each peak (p1, p2, and p3) among those automatically detected at curve inflections. Researchers cross-validated their results and, if necessary, they harmonized them using the annotation of the previous and following pulses as reference. For a few difficult cases where the researchers could not agree on the position of some peaks, the pulse was removed from the dataset. This procedure ensured that the groundtruth is not biased to a specific researcher. A custom-made annotation tool allowed for flagging missing peaks. Within our dataset, p_1 was missed in $1,717$ pulses, p_2 was missed in 265 pulses, and p_3 was missed in 34 pulses. Data from two patients was removed due to the device malfunction. The data was acquired at the Ronald Reagan medical center at the University of California, Los Angeles (UCLA) and the UCLA Internal Review Board (IRB) approved the usage of this archived dataset.

2) Simulated dataset: To verify the effectiveness of the peak detection algorithms under controlled variability, we created a simulated dataset of ICP waveforms. A probabilistic generative model was used to simulate realistic shape variations of an ICP pulse. The model was formalized as a Gaussian Mixture model (GMM) composed of three Gaussian components. The Gaussian Mixture model is a linear combination of Gaussian distributions:

$$p(x) = \Sigma_{k=1}^{K} \pi_k \, \mathcal{N}(x|\mu_k, \Sigma_k) \tag{20}$$

where π_k is the weight associated with the k^{-th} component, and the number of components K was set to 3 in our experiments. The parameters π_k, μ_k, Σ_k were fitted using the clinical data using a random sample of $1,500$ ICP waveforms.

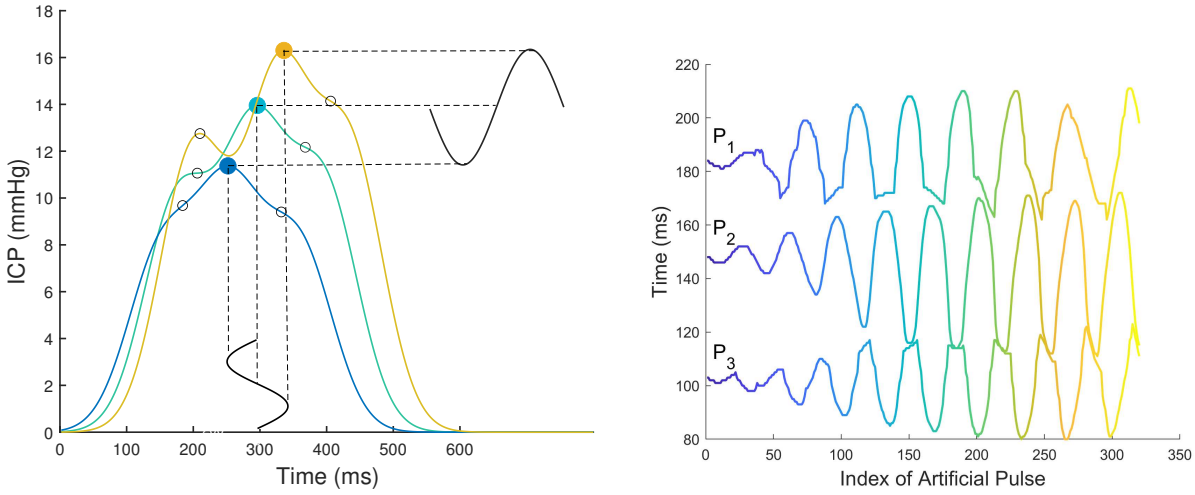

(a) (b)

Fig. 6: Illustration of simulated ICP waveforms from our GMM generative model (a) and corresponding latency for the 3 peaks (p1, p2, p3) over a sequence of generated data (b).

A series of pulses was then generated from this GMM model by incorporating an independent temporal change $c_{i\in1,2,3} = sin(z)$ on the mean of each component $\mu_k \in \mathcal{R}^2$. The model of the temporal dynamic was formalized as a sine wave function whose value c_k was added to its corresponding mean μ_k. It should be noted that two independent sine functions were used: one that acts on the latency and the other on the pressure of each peak. The generative model was then used to reconstruct individual waveform pulses at a data sampling rate is 400Hz. The range of the sine wave was constrained by the fluctuation range observed in our clinical datasets. Figure 6 illustrate the variations induced by the sine wave on the latency of the three peaks.

C. Experiments

Our experiments aim at comparing the accuracy of several machine learning models in locating the peaks within the ICP signal. For both the clinical and simulated datasets, we evaluate the accuracy of the models in detecting the peaks under a varying amount of noise. We also perform evaluations to evaluate robustness to missing data.

1) **Experiment #1: Peak Detection in Individual Waveforms:** The evaluation performed as part of this experiment is carried out on individual waveforms where the input provided to the regression model does not include any context or waveforms from previous time-points. The algorithms evaluated in our benchmark are spectral regression (SR), Kernel spectral regression (KSR), Neural networks (NN), Support vector machines (SVM), and long short-term memory models (LSTM).

A 10-fold cross-validation is performed separately on the clinical and simulated datasets. The ICP waveforms with missing peaks were included as part of the experiments. However, the missing peaks were ignored from the computation of the error. For both datasets, the input provided to the machine learning algorithms is the ICP waveform re-sampled at 400Hz. The root mean square error (RMSE) is used as metric of accuracy and computed per peak and for each algorithm,

$$RMSE = \sqrt{\frac{\sum_{i=1}^{n}(y_i - \hat{y_i})^2}{n}} \tag{21}$$

where y_i represents the i-*th* observation, $\hat{y_i}$ is the prediction of y_i for the given model, and n denotes the total number of observations. The average error is computed across the 3 peaks between the actual value of the peaks $y_i = (p_1, p_2, p_3)$ and the prediction $\hat{y_i} = (\hat{p}_1, \hat{p}_2, \hat{p}_3)$ of the regression method.

The monitoring of ICP can be adversely impacted by various noise and artifacts (including electromagnetic interference from other equipment, and self-noise). In practice, it is manifested by abnormal fluctuations in the ICP waveform. To reflect these signal perturbations and evaluate the robustness of peak detection algorithm to them, we create noisy replication of our ICP datasets by adding varying levels of noise (from 5 to 15%) on the original ICP waveform.

2) **Experiment #2: Peak detection in Continuous ICP:** In this second experiment, the evaluation is conducted on a series of ICP pulses. In particular, we assume that a regression algorithms first predicts the position of the 3 peaks. Such prediction, which is affected by noise and artifacts, is then filtered using a trakcking algorithm to obtain a refined position

of the peaks by utilizing temporal dependencies between succesive ICP pulses. The tracking algorithms evaluated are MOCAIP, Nonparametric Bayesian tracking, Kalman filter, and LSTM. The regression model used to obtained candidate peaks on single waveforms is KSR. Similarly to our previous experiment, we repeat the evaluation by adding various levels of noise (5 to 15%) to the simulated data.

In some cases, the patients movement or other physiological activities will cause loss of connectivity, resulting in data loss in the ICP waveform. In the absence of signal, traditional ICP peak detection algorithms based on a single waveform will fail. To simulate this situation, we modified the simulated dataset such that some intervals are set to null. This helps verify whether tracking algorithm can utilize prior information to keep track of the peak over time. To simulate the missing ICP waveform, we divide the simulated waveform into several groups, and two or three missing segments of various lengths (2 to 4 pulses missing) are produced in each group to ensure the randomness of the missing situation and the dispersion of its distribution in the whole waveform.

DECLARATIONS

D. Ethical Approval

The data was acquired at the Ronald Reagan medical center at the University of California, Los Angeles (UCLA) and the UCLA Internal Review Board (IRB) approved the usage of this archived dataset.

E. Competing interests

Not applicable.

F. Authors' contributions

M.W. and F.S. wrote the main manuscript text and M.W., F.S., S.S., and S.K. prepared figures and literature review. All authors reviewed the manuscript.

G. Funding

Prof. Miaomiao Wei was supported by a grant from the China Scholarship Council.

H. Availability of data and materials

Data and code to replicate experiments will be made available on Prof. Fabien Scalzo's website http://www.fabiens.net.

REFERENCES

[1] E. R. Cardoso, J. O. Rowan, and S. Galbraith, "Analysis of the cerebrospinal fluid pulse wave in intracranial pressure," *J Neurosurg*, vol. 59, no. 5, pp. 817–21, 1983.

[2] E. R. Cardoso, K. Reddy, and D. Bose, "Effect of subarachnoid hemorrhage on intracranial pulse waves in cats," *J Neurosurg*, vol. 69, no. 5, pp. 712–8, 1988.

[3] C. F. Contant, C. S. Robertson, J. Crouch, S. P. Gopinath, R. K. Narayan, and R. G. Grossman, "Intracranial pressure waveform indices in transient and refractory intracranial hypertension," *J Neurosci Methods*, vol. 57, no. 1, pp. 15–25, 1995.

[4] H. Takizawa, T. Gabra-Sanders, and J. D. Miller, "Changes in the cerebrospinal fluid pulse wave spectrum associated with raised intracranial pressure," *Neurosurgery*, vol. 20, no. 3, pp. 355–61, 1987.

[5] H. D. Portnoy and M. Chopp, "Cerebrospinal fluid pulse wave form analysis during hypercapnia and hypoxia," *Neurosurgery*, vol. 9, no. 1, pp. 14–27, 1981.

[6] M. Chopp and H. D. Portnoy, "Systems analysis of intracranial pressure. comparison with volume-pressure test and csf-pulse amplitude analysis," *J Neurosurg*, vol. 53, no. 4, pp. 516–27, 1980.

[7] M. Balestreri, M. Czosnyka, L. Steiner, E. Schmidt, P. Smielewski, B. Matta, and J. Pickard, "Intracranial hypertension: what additional information can be derived from ICP waveform after head injury?" *Acta Neurochir (Wien)*, vol. 146, no. 2, pp. 131–141, Feb. 2004.

[8] M. Czosnyka, E. Guazzo, M. Whitehouse, P. Smielewski, Z. Czosnyka, P. Kirkpatrick, S. Piechnik, and J. Pickard, "Significance of intracranial pressure waveform analysis after head injury," *Acta Neurochir (Wien)*, vol. 138, no. 5, pp. 531–41, 1996.

[9] C. Park, S. J. Ryu, B. H. Jeong, S. P. Lee, C. Hong, Y. B. Kim, and B. Lee, "Real-time noninvasive intracranial state estimation using unscented kalman filter," *IEEE Transactions on Neural Systems and Rehabilitation Engineering*, vol. 27, no. 9, pp. 1931–1938, 2019.

[10] S. Asgari, N. K. Arevalo, R. Hamilton, D. Hanchey, and F. Scalzo, "Cerebral blood flow velocity pulse onset detection using adaptive thresholding," in *2017 IEEE EMBS International Conference on Biomedical Health Informatics (BHI)*, 2017, pp. 377–380.

[11] S. Kim, R. Hamilton, S. Pineles, M. Bergsneider, and X. Hu, "Noninvasive intracranial hypertension detection utilizing semisupervised learning," *IEEE Transactions on Biomedical Engineering*, vol. 60, no. 4, pp. 1126–1133, 2013.

[12] S. L. Oh, E. Y. Ng, R. S. Tan, and U. R. Acharya, "Automated diagnosis of arrhythmia using combination of cnn and lstm techniques with variable length heart beats," *Computers in Biology and Medicine*, vol. 102, pp. 278 – 287, 2018. [Online]. Available: http://www.sciencedirect.com/science/article/abs/pii/S0010482518301446

[13] X. Hu, T. Glenn, F. Scalzo, M. Bergsneider, C. Sarkiss, N. Martin, and P. Vespa, "Intracranial pressure pulse morphological features improved detection of decreased cerebral blood flow," *Physiological Measurement*, vol. 31, no. 5, pp. 679–695, mar 2010. [Online]. Available: https://doi.org/10.1088%2F0967-3334%2F31%2F5%2F006

[14] A. L. Jacobson, "Auto-threshold peak detection in physiological signals," in *2001 Conference Proceedings of the 23rd Annual International Conference of the IEEE Engineering in Medicine and Biology Society*, vol. 3, 2001, pp. 2194–2195 vol.3.

[15] A. Kaur, R. Agarwal, and A. Kumar, "Adaptive threshold method for peak

detection of surface electromyography signal from around shoulder muscles," *Journal of Applied Statistics*, vol. 45, no. 4, pp. 714–726, 2018. [Online]. Available: https://doi.org/10.1080/02664763.2017.1293624

[16] R. Slodzinski, L. Hildebrand, and W. Vautz, *Peak Detection Algorithm Based on Second Derivative Properties for Two Dimensional Ion Mobility Spectrometry Signals*. Berlin, Heidelberg: Springer Berlin Heidelberg, 2013, pp. 341–354. [Online]. Available: https://doi.org/10.1007/978-3-642-34471-8_28

[17] A. Kumar, R. Ranganatham, R. Komaragiri, and M. Kumar, "Efficient qrs complex detection algorithm based on fast fourier transform," *Biomedical engineering letters*, vol. 9, no. 1, p. 145151, February 2019. [Online]. Available: https://europepmc.org/articles/PMC6431324

[18] H. Rabbani, M. P. Mahjoob, E. Farahabadi, and A. Farahabadi, "R peak detection in electrocardiogram signal based on an optimal combination of wavelet transform, hilbert transform, and adaptive thresholding," *Journal of medical signals and sensors*, vol. 1, no. 2, p. 9198, May 2011.

[19] H. Chen and K. Maharatna, "An automatic r and t peak detection method based on the combination of hierarchical clustering and discrete wavelet transform," *IEEE Journal of Biomedical and Health Informatics*, vol. 24, no. 10, pp. 2825–2832, 2020.

[20] K. H. Jarman, D. S. Daly, K. K. Anderson, and K. L. Wahl, "A new approach to automated peak detection," *Chemometrics and Intelligent Laboratory Systems*, vol. 69, no. 1, pp. 61–76, 2003. [Online]. Available: https://www.sciencedirect.com/science/article/abs/pii/S0169743903001138

[21] T. Chanwimalueang, W. von Rosenberg, and D. P. Mandic, "Enabling r-peak detection in wearable ecg: Combining matched filtering and hilbert transform," in *2015 IEEE International Conference on Digital Signal Processing (DSP)*, 2015, pp. 134–138.

[22] T. Nguyen, X. Qin, A. Dinh, and F. Bui, "Low resource complexity r-peak detection based on triangle template matching and moving average filter," *Sensors*, vol. 19, no. 18, 2019. [Online]. Available: https://www.mdpi.com/1424-8220/19/18/3997

[23] M. I. Sezan, "A peak detection algorithm and its application to histogram-based image data reduction," *Computer Vision, Graphics, and Image Processing*, vol. 49, no. 1, pp. 36–51, 1990. [Online]. Available: https://www.sciencedirect.com/science/article/pii/0734189X9090161N

[24] B. Halder, S. Mitra, and M. Mitra, "Detection and identification of ecg waves by histogram

approach," in *2016 2nd International Conference on Control, Instrumentation, Energy Communication (CIEC)*, 2016, pp. 168–172.

[25] S. Farashi, "A multiresolution time-dependent entropy method for qrs complex detection," *Biomedical Signal Processing and Control*, vol. 24, pp. 63–71, 2016. [Online]. Available: https://www.sciencedirect.com/science/article/pii/S1746809415001561

[26] K. Harmer, G. Howells, W. Sheng, M. Fairhurst, and F. Deravi, "A peak-trough detection algorithm based on momentum," in *2008 Congress on Image and Signal Processing*, vol. 4, 2008, pp. 454–458.

[27] H. Deng, B. Xiang, X. Liao, and S. Xie, "A linear modulation-based stochastic resonance algorithm applied to the detection of weak chromatographic peaks," *Analytical and Bioanalytical Chemistry*, vol. 386, no. 7-8, pp. 2199–2205, 2006.

[28] K. I. Panoulas, L. J. Hadjileontiadis, and S. M. Panas, "Enhancement of r-wave detection in ecg data analysis using higher-order statistics," in *2001 Conference Proceedings of the 23rd Annual International Conference of the IEEE Engineering in Medicine and Biology Society*, vol. 1, 2001, pp. 344–347 vol.1.

[29] L. EL BOUNY, M. KHALIL, and A. ADIB, "Qrs complex detection based on smoothed nonlinear energy operator," in *2018 9th International Symposium on Signal, Image, Video and Communications (ISIVC)*, 2018, pp. 191–196.

[30] M. B. Hossain, S. K. Bashar, A. J. Walkey, D. D. McManus, and K. H. Chon, "An accurate qrs complex and p wave detection in ecg signals using complete ensemble empirical mode decomposition with adaptive noise approach," *IEEE Access*, vol. 7, pp. 128 869–128 880, 2019.

[31] L. El Bouny, M. Khalil, and A. Adib, "R peak detection based on wavelet transform and nonlinear energy operator," in *Smart Data and Computational Intelligence*, F. Khoukhi, M. Bahaj, and M. Ezziyyani, Eds. Cham: Springer International Publishing, 2019, pp. 104–112.

[32] T. Dave and U. Pandya, "R peak detection for wireless ecg using dwt and entropy of coefficients," *International Journal of Biomedical Engineering and Technology*, vol. 34, no. 3, pp. 268–283, 2020. [Online]. Available: https://www.inderscienceonline.com/doi/abs/10.1504/IJBET.2020.111472

[33] D. Cai, X. He, and J. Han, "SRDA: An Efficient Algorithm for Large-Scale Discriminant Analysis," *IEEE Trans Knowl Data Eng*, vol. 20, no. 1, pp. 1–12, 2008.

[34] M. A. Hasan, M. B. I. Reaz, and M. I. Ibrahimy, "Fetal electrocardiogram extraction and r-peak detection for fetal heart rate monitoring using artificial neural network and correlation," in *The 2011 International Joint Conference on Neural Networks*, 2011, pp. 15–20.

[35] C.-C. Chang and C.-J. Lin, *LIBSVM: a library for support vector machines*, 2001, software available at http://www.csie.ntu.edu.tw/~cjlin/libsvm.

[36] P. Geurts, D. Ernst, and L. Wehenkel, "Extremely randomized trees," *Mach Learn*, vol. 63, no. 1, pp. 3–42, 2006.

[37] M. Hagan and M. Menhaj, "Training feedforward networks with the marquardt algorithm," *IEEE Transactions on Neural Networks*, vol. 5, no. 6, pp. 989–993, 1994.

[38] M. Akhbari, M. Niknazar, C. Jutten, M. B. Shamsollahi, and B. Rivet, "Fetal electrocardiogram r-peak detection using robust tensor decomposition and extended kalman filtering," in *Computing in Cardiology 2013*, 2013, pp. 189–192.

[39] F. Scalzo, S. Asgari, S. Kim, M. Bergsneider, and X. Hu, "Bayesian tracking of intracranial pressure signal morphology," *Artificial Intelligence in Medicine*, vol. 54, no. 2, pp. 115–123, 2012. [Online]. Available: https://doi.org/10.1016/j.artmed.2011.08.007

[40] S. Hochreiter and J. Schmidhuber, "Long Short-Term Memory," *Neural Computation*, vol. 9, no. 8, pp. 1735–1780, 11 1997. [Online]. Available: https://doi.org/10.1162/neco.1997.9.8.1735

[41] X. Hu, P. Xu, F. Scalzo, P. Vespa, and M. Bergsneider, "Morphological Clustering and Analysis of Continuous Intracranial Pressure," *IEEE Trans Biomed Eng*, vol. 56, no. 3, pp. 696–705, 2009.

[42] G. Welch and G. Bishop, "An introduction to the kalman filter," USA, Tech. Rep., 1995.

[43] E. B. Sudderth, A. T. Ihler, M. Isard, W. T. Freeman, and A. S. Willsky, "Nonparametric belief propagation," *Commun. ACM*, vol. 53, no. 10, p. 95103, Oct. 2010. [Online]. Available: https://doi.org/10.1145/1831407.1831431

[44] X. Hu, P. Xu, D. Lee, P. Vespa, and M. Bergsneider, "An algorithm of extracting intracranial pressure latency relative to electrocardiogram r wave," *Physiol Meas*, vol. 29, pp. 459–471, 2008.

[45] V. X. Afonso, W. J. Tompkins, T. Q. Nguyen, and S. Luo, "Ecg beat detection using filter banks," *IEEE Trans Biomed Eng*, vol. 46, no. 2, pp. 192–202, 1999.